



# Cubic group-III nitride-based nanostructures—basics and applications in optoelectronics

D.J. As

Department of Physics, University of Paderborn, Warburger Strasse 100, 33098 Paderborn, Germany

## ARTICLE INFO

Available online 12 September 2008

### Keywords:

Cubic group-III nitrides  
MBE  
Intersubband absorption  
Cubic HFETs

## ABSTRACT

Molecular beam epitaxy (MBE) of cubic group-III nitrides is a direct way to eliminate the polarization effects which inherently limits the performance of optoelectronic devices containing quantum well or quantum dot active regions. In this contribution the latest achievement in the MBE of phase-pure cubic GaN, AlN, InN and their alloys will be reviewed. A new reflected high-energy electron beam (RHEED) control technique enables to carefully adjust stoichiometry and to severely reduce the surface roughness, which is important for any hetero-interface. The structural, optical and electrical properties of cubic nitrides and AlGaIn/GaN will be presented. We show that no polarization field exists in cubic nitrides and demonstrate 1.55  $\mu\text{m}$  intersubband absorption in cubic AlN/GaN superlattices. Further the progress towards the development and fabrication of cubic hetero-junction field effect transistors (HFETs) is discussed.

© 2008 Elsevier Ltd. All rights reserved.

## 1. Introduction

State-of-the-art group-III nitride-based electronic and optoelectronic devices based on nitride films are grown along the polar *c*-direction, which suffer from the existence of strong “built-in” piezoelectric and spontaneous polarization. This inherent polarization limits the performance of optoelectronic devices containing quantum well (QW) or quantum dot active regions. To get around this problem much attention has been focused on the growth of non- or semi-polar (Al, Ga, In)N in the last few years. However, the direct way to eliminate polarization effects will be to use non-polar (001)-oriented zinc-blend III nitride layers. With cubic epilayers, a direct transfer of the existing GaAs technology to cubic III nitrides will be possible and the fabrication of diverse electronics and optoelectronic devices will be facilitated. In this paper the latest achievement in the molecular beam epitaxy (MBE) of phase-pure cubic GaN, AlN, InN and their application in optoelectronic devices will be reviewed.

## 2. Experiment

Cubic group-III nitride samples were grown on 200  $\mu\text{m}$  thick, free standing 3C-SiC (001) substrates by MBE [1,2]. An Oxford Applied Research HD25 radio frequency plasma source was used to provide activated nitrogen atoms. Indium, aluminum and gallium were evaporated from Knudsen cells. Prior to growth,

the 3C-SiC substrates were chemically etched by organic solvents and a buffered oxide etch (BOE) and annealed for 10 h at 500 °C. Cubic GaN layers were deposited at 720 °C directly on 3C-SiC substrates. The adsorption and desorption of metal (Ga) layers on the *c*-GaN surface was investigated using the intensity of a reflected high-energy electron beam (RHEED) as a probe. The structural and morphological properties of both the 3C-SiC substrates and the group-III nitride epilayers were measured by high-resolution X-ray diffraction (HRXRD) and atomic force microscopy (AFM). Reciprocal space mapping (RSM) have been performed to determine the Al and In molar fraction and the strain in the epilayers.

## 3. Results and discussion

### 3.1. RHEED control

As an important step to improve the GaN surface morphology in a systematic way, it is essential to understand the surface structure and the underlying growth process on an atomic scale. In particular, the kinetic processes of adsorption and desorption on the surface are considered as key parameters that govern the surface morphology, incorporation kinetics and consecutively the overall material quality. In MBE of GaN, two dimensional surfaces are commonly achieved under Ga-rich conditions, with theoretical [3] and experimental [4,5] evidence suggesting that the growth front is stabilized by a metallic Ga adlayer. The optimum conditions for the epitaxial growth of *c*-GaN are mainly determined by two parameters, the surface stoichiometry and the

E-mail address: [d.as@upb.de](mailto:d.as@upb.de)

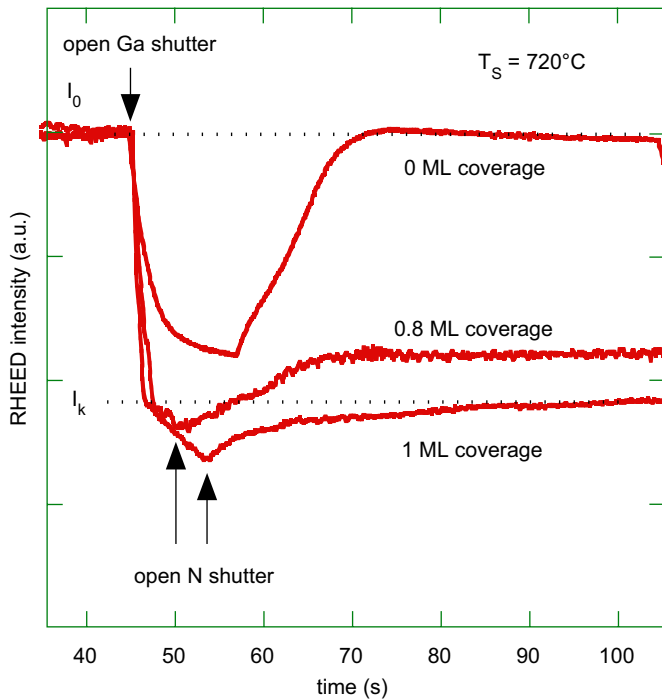


**Fig. 1.** RHEED intensity transient measured during the growth of c-GaN, which started after opening the N source. The RHEED intensity measured during growth yields the amount of excess Ga (indicated in the figure) on the c-GaN surface. The Ga fluxes are  $4.4 \times 10^{14}$ ,  $3.2 \times 10^{14}$ , and  $1.2 \times 10^{14} \text{ cm}^{-2}$  for the coverages of 1, 0.8, and 0 ML, respectively.

substrate temperature [1]. Both parameters are interrelated; therefore an in-situ control of substrate temperature and surface stoichiometry is highly desirable. The study of the surface reconstruction by RHEED was one of the key issues in understanding the c-III nitride growth [1,6,7]. First principle calculations by Neugebauer et al. [8] show that all energetically favoured surface modifications of the non-polar (001) c-GaN surface are Ga-stabilized and therefore optimum growth conditions are expected under slightly Ga-rich conditions.

Fig. 1 shows the RHEED intensity transient of the (0,0) reflection of the  $(2 \times 2)$  reconstruction. After opening the Ga shutter we observe a steep linear decrease of the RHEED intensity between  $I_0$  and the kink position ( $I_k$ ). The gradient of the intensity drop is related to the impinging Ga flux. Using the known value of the Ga flux and the time  $\Delta t_k$  it takes for the RHEED intensity to drop to  $I_k$ , we are able to calculate the amount of adsorbed gallium. Neglecting re-evaporation of Ga we get a total number of adsorbed Ga atoms from the flux time  $\Delta t_k$  product. In all cases this product is about  $9.8 \times 10^{14} \text{ cm}^{-2}$ , which is equal the number of atoms of exactly one monolayer of Ga on the GaN surface (lattice constant of  $4.52 \text{ \AA}$ ). Since  $I_0$  is the reflectivity of the GaN surface and  $I_k$  is the reflectivity of GaN covered by one Ga monolayer, and the drop of the RHEED intensity in the time interval  $\Delta t_k$  is linear, the Ga coverage between 0 and one monolayer can be inferred from the measured intensity drop by linear interpolation. The decrease of the RHEED intensity below  $I_k$  is most likely due to further accumulation of Ga and thereby a modification of the Ga adlayer surface, however it is not proportional to the amount of adsorbed Ga. For this reason our method can only be used to measure the Ga coverage between zero and one monolayer, respectively. For Ga fluxes less than  $3 \times 10^{14} \text{ cm}^{-2} \text{ s}^{-1}$  the situation is different. For these fluxes it is not possible to define a kink position. The RHEED intensity drops to a certain value and saturates. We suppose that then desorption of Ga cannot be further neglected.

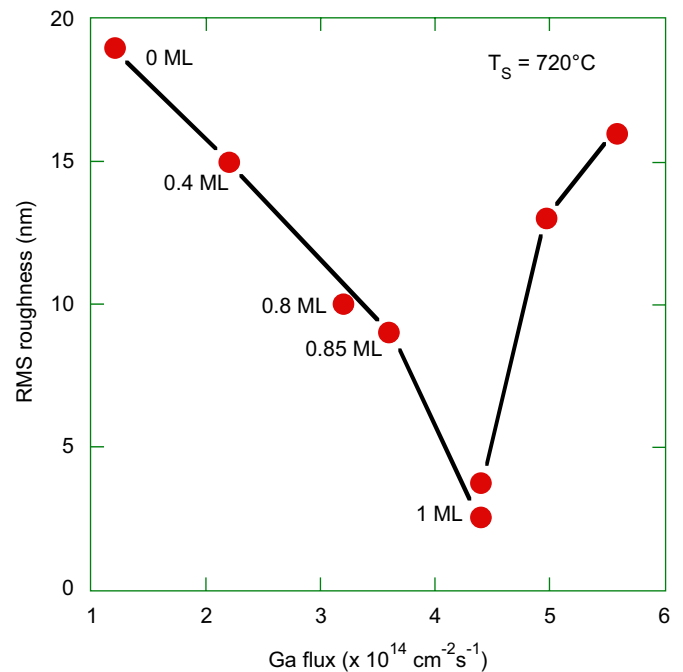


**Fig. 2.** RMS roughness of c-GaN layers measured by  $5 \times 5 \mu\text{m}^2$  AFM scans vs. Ga flux during growth. The corresponding values of the Ga coverage during growth are also included. Minimum roughness is obtained with an excess coverage of 1 ML. The line is a guide for the eyes.

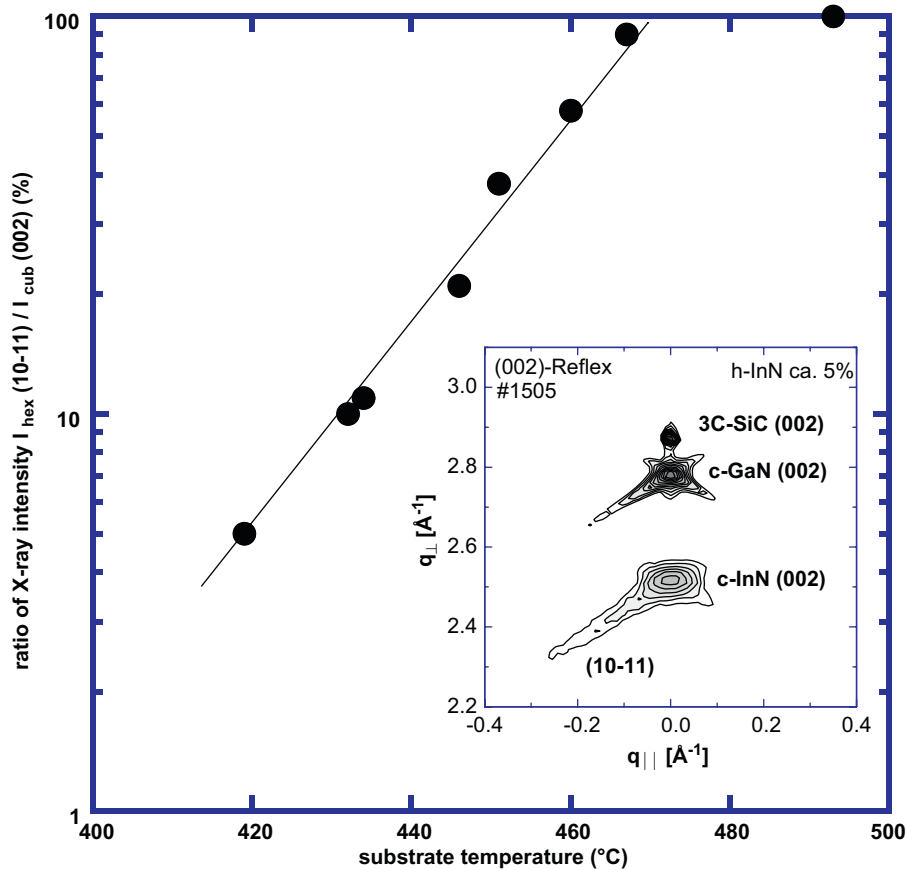
After opening the N shutter we observe an increase of the RHEED intensity which is due to the formation of c-GaN. During further growth the RHEED intensity saturates. From the saturation value the Ga coverage can be calculated using  $I_k$  as a reference. This procedure allows measuring the Ga coverage in the range between 0 and 1 monolayer with an accuracy of 0.1 monolayer.

Fig. 2 shows the root-mean-square (RMS)-roughness measured by a  $5 \times 5 \mu\text{m}^2$  AFM-scan of several c-GaN layers versus the Ga flux used during MBE. The nitrogen flux was kept constant for all samples. The corresponding values of the Ga coverage during growth, as measured by the procedure described above, are included in Fig. 2. Only values below one monolayer can be measured. Minimum roughness is obtained with one monolayer Ga coverage during growth. This is in contrast to what has been observed with h-GaN, where the optimum growth conditions with regard to surface morphology are related to the formation of a Ga bilayer (c-plane, [9,10]) or a trilayer (m-plane, [5]), respectively.

It has variously been suggested that excess Ga acts as surfactant during the epitaxy of hexagonal-GaN [9,11,12]. We believe that our data shown in Fig. 2 clearly demonstrate that this effect exists also on the (001) surface of c-GaN. The width of the (002) X-ray rocking curve measured in double axis configuration of  $1 \mu\text{m}$  thick c-GaN layers grown with one monolayer coverage is about 16 arcmin. Among our c-GaN layers with equal thickness 16 arcmin is a minimum value. Gallium fluxes which are equivalent to a Ga coverage exceeding one monolayer lead to a pronounced increase of the roughness and the full width at half maximum (FWHM) of the X-ray rocking curve.

### 3.2. Cubic InN

Among nitride semiconductors, InN is the least investigated of all and is expected to be a promising material for high frequency



**Fig. 3.** Intensity ratio of the  $(10\bar{1}1)$  reflex of hexagonal inclusions to the  $(002)$  Bragg reflex of cubic InN versus growth temperature of c-InN layers. The inset shows the reciprocal space map for the c-InN sample grown at  $419^\circ\text{C}$ .

electronic devices [13,14]. The most important recent discovery about InN is that it has a much narrower band-gap than reported previously. For h-InN, values between 0.6 and 0.7 eV are measured [15,16]. Group-III nitrides with cubic crystal structure are expected to have even lower band-gaps and can be grown on substrates with cubic structure. However, the zinc-blende polytype is metastable and only a very narrow growth window is available for the process conditions [1].

Cubic InN films were grown on top of a c-GaN buffer layer (600 nm). The c-GaN buffer layer was deposited on free standing 3C-SiC (001) substrates at growth temperatures of  $720^\circ\text{C}$ . For the InN growth the temperature was reduced and varied in the range  $419\text{--}490^\circ\text{C}$ . InN growth was started under In-rich conditions at an In-BEP of  $6.8 \times 10^{-8}$  mbar and was decreased to  $3.1 \times 10^{-8}$  mbar after two minutes of growth. The thicknesses of the InN layers were at least 130 nm and the growth was continuously monitored by RHEED.

HRXRD investigations were performed to determine the phase purity of our c-InN layers. All  $\omega$ - $2\theta$ -scans confirmed the formation of the cubic phase of InN. Bragg peaks observed at  $35.8^\circ$ ,  $39.9^\circ$  and  $41.3^\circ$  correspond to c-InN (002), c-GaN (002) and 3C-SiC (002), respectively. No additional reflection of h-InN grown in (002) direction was detected. The FWHM of the (002) rocking curve was 48 arcmin. The lattice constant derived from the  $\omega$ - $2\theta$ -scan is  $5.01 \pm 0.01 \text{ \AA}$  in good agreement to the values published [9]. However, it is well known that hexagonal inclusions mainly grow on (111) facets and cannot be detected by  $\omega$ - $2\theta$ -scans. Therefore reciprocal space maps (RSM) of the GaN (002) Bragg-reflex were performed. The RSM along the  $(\bar{1}10)$  azimuth is shown in the inset of Fig. 3. The growth temperature of this InN

sample was  $419^\circ\text{C}$ . From the intensity ratio of the cubic (002) reflex to the hexagonal  $(10\bar{1}1)$  reflex we estimate 95% cubic phase in this InN layer. RSM of the asymmetric GaN  $(\bar{1}\bar{1}3)$  reflex show, that the lattice of our c-InN layers is fully relaxed with respect to the c-GaN buffer.

In Fig. 3 we plot the ratio of the intensities of the h- $(10\bar{1}1)$  Bragg reflex and the c-(002) reflex versus the growth temperature of different InN layers. We observe a strong decrease of hexagonal inclusions with decreasing growth temperature up to a minimum value of 5%. This supports the idea that with decreasing growth temperature the sticking coefficient of In is increased, resulting in a higher density of cubic nuclei on the surface, which reduce the formation of (111) facets.

The low-temperature photoluminescence (PL) spectrum of an InN layer grown at  $419^\circ\text{C}$  shows a peak at about 0.69 eV with a FWHM of 170 meV [17]. We suppose that the broadening of the luminescence is due to the fact that the c-InN is degenerated. The high electron densities above  $10^{19} \text{ cm}^{-3}$  cause pronounced Burstein–Moss shifts at the gap. Taking into account non-parabolicity and band filling effects, data analysis yields renormalized band edges  $E_g(n)$  close to 0.61 eV at low temperature for c-InN. Subtracting a temperature shift of about 50 meV between 10 and 300 K the band-gap of c-InN is about 0.56 eV at room temperature. This value is in excellent agreement with measurements of the complex dielectric function for cubic InN by spectroscopic ellipsometry (SE) from the mid-infrared into the visible spectral region. From SE a zero-density band-gap of  $\approx 0.595 \text{ eV}$  is estimated for c-InN. Therefore, the band-gap of cubic InN is about 85 meV lower than that for hexagonal InN [18].

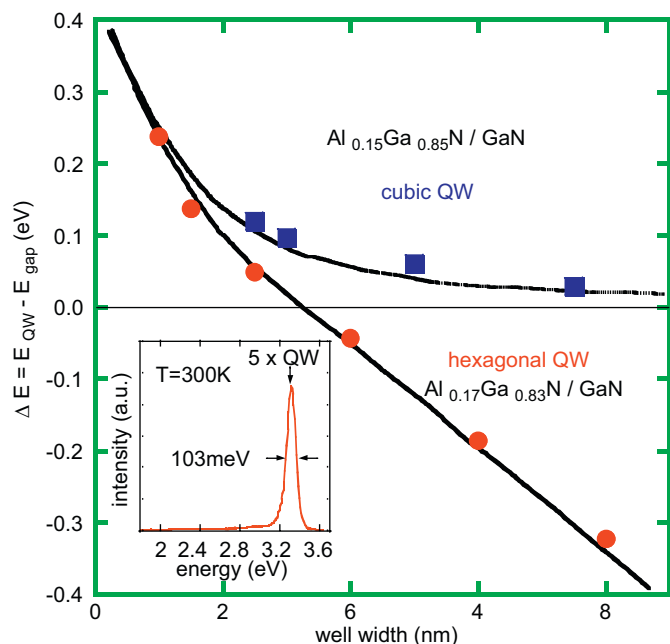


**Fig. 4.** Transition energies of  $\text{Al}_{0.15}\text{Ga}_{0.85}\text{N}/\text{GaN}$  MQWs versus well width for cubic (squares) and hexagonal (dots) MQWs. The squares and dots are experimental data; the curves are calculated using a self-consistent Poisson–Schrödinger model. For the hexagonal QWs an internal field of 750 kV/cm is estimated. Inset: Room temperature PL spectrum of a cubic MQW.

A pronounced difficulty in the determination of the electrical properties of InN is due to the fact that electron accumulation is found to occur at the surface of wurtzite InN. Using X-ray photoemission spectroscopy a similar accumulation effect is also demonstrated for cubic InN [19]. The surface Fermi level pinning was shown to be the same for *a*-plane and for both polarities of *c*-plane wurtzite InN, although the pinning was slightly lower for zinc-blende (001) InN. This is due to the low  $\Gamma$ -point conduction band minimum lying significantly below the charge neutrality level. Therefore, the accumulation is shown to be a universal feature of InN surfaces.

### 3.3. Cubic AlGaIn/GaN QW structures

To demonstrate the absence of internal spontaneous polarization fields in the cubic group-III nitrides cubic single and multiple  $\text{Al}_{0.15}\text{Ga}_{0.85}\text{N}/\text{GaN}$  QWs were grown on 3C-SiC/GaN substrates [20]. The quantum structures consist of 6 nm thick  $\text{Al}_{0.15}\text{Ga}_{0.85}\text{N}$  barriers and GaN wells with a width of 2.5–7.5 nm and were sandwiched between 50 nm AlGaIn cladding layers. During the growth of  $\text{Al}_{0.15}\text{Ga}_{0.85}\text{N}/\text{GaN}$  QWs clear RHEED oscillations were observed allowing a stringent control of the growth rate and indicating two dimensional growth of the respective layers. The room temperature PL spectra of a multiple quantum well (MQW) structure excited with a HeCd-UV laser is shown in the inset of Fig. 4. The dimensions of the quantum structures are 3 nm thick wells and 6 nm barriers. We observe a strong emission at 3.30 eV, which lies between the *c*-GaN emission at 3.2 eV and the emission of the  $\text{Al}_{0.15}\text{Ga}_{0.85}\text{N}$  cladding layer at about 3.48 eV [21]. The PL linewidth of cubic QW luminescence is about 103 meV and is almost comparable to values reported for non-polar hexagonal AlGaIn/GaN QWs [22]. We attribute the slightly broader linewidth in the cubic structures to the higher density of dislocations.

Fig. 4 depicts the dependency of the QW emission energy on the well width for both cubic (blue squares) and hexagonal QWs (red dots). Therein, the shift in transition energies compared to

the band-gap energy is plotted versus well width. For our cubic  $\text{Al}_{0.15}\text{Ga}_{0.85}\text{N}/\text{GaN}$  QWs the peak energy of the emission exactly follows the square-well Poisson–Schrödinger model and demonstrates the absence of polarization induced electrical fields. For comparable hexagonal  $\text{Al}_{0.17}\text{Ga}_{0.83}\text{N}/\text{GaN}$  QWs on sapphire substrates the experimental data can only be explained if an internal spontaneous electrical field of 750 kV/cm has been taken into account [23]. These results indicate that the well known thermodynamic metastability of the cubic nitrides does not necessarily limit their application for polarization free structures.

### 3.4. Intersubband transitions

Intersubband transitions form the basis for quantum well infrared photodetectors (QWIP) and quantum cascade lasers (QCL). Due to the wide band-gaps and the large band offsets between AlN and GaN this group of III-nitrides offer intersubband transitions in the technologically important infrared 1.3–1.5  $\mu\text{m}$  spectral range. The growth of non-polar cubic GaN/AlN MQW structures on (001) oriented substrates will eliminate the detrimental strong spontaneous polarization fields, allowing easier design of the complex MQW structures with various QW widths as it is necessary for the QCL systems.

Cubic GaN/AlN short period MQW structures were grown at 720 °C by using plasma-assisted MBE on free standing 3C-SiC substrates [24]. The buffer layer was chosen as 100 nm thick GaN and the active region is composed of 20 periods of  $L_W$  GaN/1.5 nm AlN, where  $L_W$  is the well thickness and it was chosen between 1.6–2.10 nm. The active region is then capped by a 100 nm thick GaN. The structural properties were measured by HRXRD. From the difference of the superlattice peaks in the  $\omega$ - $2\theta$ -scan of the (002) reflection a periodicity of 3.1 nm was estimated by using a dynamic simulation program for a 20 period GaN/AlN MQW structure. From the knowledge of the growth rates of AlN and GaN, obtained from RHEED oscillations, a barrier and well width of 1.35 and 1.75 nm is determined, respectively.

In Fig. 5 the optical absorption spectra of the intersubband transitions measured at room temperature is shown for four different MQW samples with well widths ranging between 1.60 and 2.10 nm, respectively. All four samples exhibit strong absorption peaks in the spectral range of 1.5–2  $\mu\text{m}$ . In the inset of Fig. 5 the measured intersubband transition peak position energies (red circles) and the calculated (solid black line) transition energies using a square well self-consistent Poisson–Schrödinger model is depicted. It is clear from this figure that good agreement is obtained between theory and experiment.

Recently, photodetectors based on intersubband transitions in molecular beam epitaxially grown cubic GaN/AlN MQWs were fabricated and tested [25]. The samples were polished into waveguide configuration on which the devices were fabricated and the photoresponse spectra were collected in the temperature range of 77–215 K under the influence of small bias voltages. All devices exhibit photovoltaic effect where the photoresponse is observed at zero bias voltage.

### 3.5. Cubic hetero-field effect transistors

AlGaIn/GaN hetero-junction field effect transistors (HFETs) are presently of outstanding interest for electronic devices, in particular, for high-power and high-frequency amplifiers. This is motivated by the potential commercial and military field application, namely, in the area of communication systems, radar, wireless stations, high-temperature electronics and high-power solid-state switching [26,27]. Standard HFETs were realized with h-III-nitrides, where at the interface of h-AlGaIn/GaN hetero-structures a 2DEG is formed due to strong inherent polarization

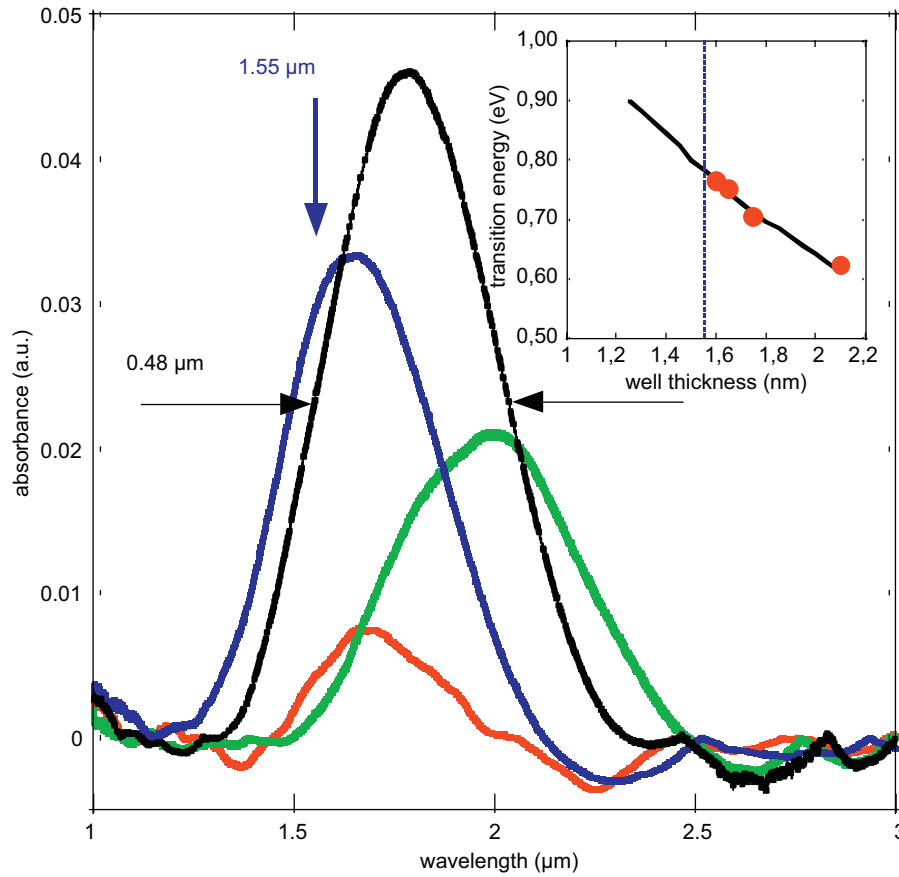


Fig. 5. Optical absorption spectra of the intersubband transitions in cubic GaN/AlN short period MQWs. Inset: Intersubband transitions energy vs. well width. Circles are the experimental data and the solid line is the results of the theoretical calculations.

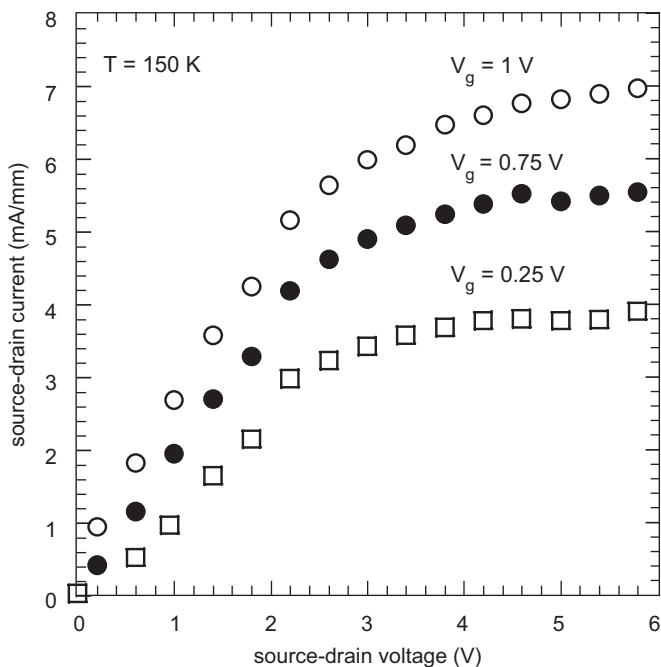


Fig. 6.  $I_{DS}$ – $V_{DS}$  characteristics of cubic AlGaIn/GaN HFET ( $W_g/L_g = 100/6 \mu\text{m}$ ) measured at 150 K after subtraction of the c-GaN buffer conductivity.

available. Recently, simulation data on cubic AlGaIn/GaN HFETs on 3C-SiC substrates clearly show that normally-off mode operation could be realized with the large technological allowance and the same flexible design ability as GaAs/AlGaAs HFET technology [28].

First, c-AlGaIn/GaN based HFET structures were fabricated on 3C-SiC (001) substrates.  $C$ – $V$  measurements at  $T = 150\text{ K}$  clearly prove the existence of a 2DEG and a sheet carrier concentration of about  $1.6 \times 10^{12} \text{ cm}^{-2}$  is measured at the interface in good agreement with numerical simulation [29]. Analysis of the  $I$ – $V$  characteristic of the gate contact at 150 K revealed a rectifying behavior of the Schottky contact. The  $I_{SD}$ – $V_{SD}$  characteristics measured at 150 K exhibited a clear field effect of  $I_{SD}$  induced by applying a gate voltage between +0.25 and +1 V (Fig. 6). However, a strong influence of the conductive GaN buffer on the  $I_{SD}$ – $V_{SD}$  characteristics was observed indicating high parallel conductance in the underlying cubic GaN buffer and the conductive 3C-SiC substrate. Subtraction of the influence of the c-GaN buffer and 3C-SiC conductivity, a clear evidence for the current transport via a 2DEG was found, due to the saturation of  $I_{SD}$  at  $V_{SD} > 3\text{ V}$ . Although this device shows normally-on mode and operates at low temperatures, it demonstrates feasibility of cubic group-III nitrides also for electrical devices. To reach normally-off operation investigation by using C-doped cubic GaN buffer layers are currently under way.

#### 4. Conclusion

Cubic group-III nitrides grown by MBE may form the basis for future non-polar optoelectronic and electronic devices, which are not restricted by the inherent polarization effects. A new RHEED

fields. Thus, devices reported so far show normally-on mode operation. However, GaN/AlGaIn HFETs with normally-off mode operation, which are also required for some systems, are hardly

control technique enables to carefully adjust stoichiometry and to severely reduce the surface roughness. The structural, optical and electrical properties of cubic nitrides and AlGa<sub>N</sub>/Ga<sub>N</sub> are presented. We proved the absence of polarization field in cubic nitrides and demonstrated 1.55 μm intersubband absorption in cubic AlN/GaN superlattices. Feasibility of cubic group-III nitrides is shown for electrical devices (HFETs), however parasitic parallel conductance in the underlying GaN buffer and 3C-SiC still dominate the performance and have to be eliminated.

### Acknowledgements

The author wants to thank K. Lischka, S. Potthast, J. Schörmann, E. Tschumak, T. Schupp at University of Paderborn, Prof. M.O. Manasreh and E. DeCuir, Jr. at Arkansas State University, J. Gerlach at IOM Leipzig, R. Goldhahn at University of Ilmenau and T. Veal at University of Warwick. My special regards are expressed to Dr. M. Abe and Dr. H. Nagasawa at HOYA Corporation, for the supply of excellent 3C-SiC substrates and the financial support by DFG.

### References

- [1] D.J. As, in: M.O. Manasreh (Ed.), *Optoelectronic Properties of Semiconductors and Superlattices*, Vol. 19, Taylor & Francis, New York, 2003, pp. 323–450 Chapter. 9.
- [2] D.J. As, S. Potthast, J. Schörmann, S.F. Li, K. Lischka, H. Nagasawa, M. Abe, *Mater. Sci. Forum* 527 (2006) 1489.
- [3] J.E. Northrup, J. Neugebauer, R.M. Feenstra, A.R. Smith, *Phys. Rev. B* 61 (2000) 9932.
- [4] G. Koblmüller, J. Brown, R. Averbeck, H. Riechert, P. Pongratz, J.S. Speck, *Appl. Phys. Lett.* 86 (2005) 041908.
- [5] O. Brandt, Y.J. Sun, L. Däweritz, K.H. Ploog, *Phys. Rev. B* 69 (2004) 165326.
- [6] D. Schikora, M. Hankeln, D.J. As, K. Lischka, T. Litz, A. Waag, T. Buhrow, F. Henneberger, *Phys. Rev. B* 54 (1996) R8381.
- [7] G. Feuillet, H. Hamaguchi, K. Ohta, P. Hacke, H. Okumura, S. Yoshida, *Appl. Phys. Lett.* 70 (1997) 1025.
- [8] J. Neugebauer, Z. Zywiets, M. Scheffler, J.E. Northrup, C.G. Van der Walle, *Phys. Rev. Lett.* 80 (1998) 3097.
- [9] G. Mula, C. Adelmann, S. Moehl, J. Oullier, B. Daudin, *Phys. Rev. B* 64 (2001) 195406.
- [10] C. Adelmann, J. Brault, D. Jalabert, P. Gentile, H. Mariette, G. Mula, B. Daudin, *J. Appl. Phys.* 91 (2002) 9638.
- [11] N. Gogneau, E. Sarigiannidou, E. Monroy, S. Monnoye, H. Mank, B. Daudin, *Appl. Phys. Lett.* 85 (2004) 1421.
- [12] J. Neugebauer, T.K. Zywiets, M. Scheffler, J.E. Northrup, H. Chen, R.M. Feenstra, *Phys. Rev. Lett.* 90 (2003) 056101.
- [13] B.E. Fortz, S.K. O'Leary, M.S. Shur, L.F. Eastman, *J. Appl. Phys.* 85 (1999) 7727.
- [14] S.K. Pugh, D.J. Dugdale, S. Brand, R.A. Abram, *Semicond. Sci. Technol.* 14 (1999) 23.
- [15] C.S. Gallinat, G. Koblmüller, J.S. Brown, S. Bernardis, J.S. Speck, *Appl. Phys. Lett.* 89 (2006) 032109.
- [16] S.P. Fu, T.T. Chen, Y.F. Chen, *Semicond. Sci. Technol.* 21 (2006) 244.
- [17] J. Schörmann, D.J. As, K. Lischka, P. Schley, R. Goldhahn, S.F. Li, W. Löffler, M. Hetterich, H. Kalt, *Appl. Phys. Lett.* 89 (2006) 261903.
- [18] P. Schley, R. Goldhahn, C. Napierala, J. Schörmann, D.J. As, K. Lischka, M. Feneberg, K. Thonke, *Semicond. Sci. Technol.* 23 (2008) 055001.
- [19] P.D.C. King, T.D. Veal, C.F. McConville, F. Fuchs, J. Furthmüller, F. Bechstedt, P. Schley, R. Goldhahn, J. Schörmann, D.J. As, K. Lischka, D. Mutó, H. Naoi, Y. Nanishi, H. Lu, W.J. Schaff, *Appl. Phys. Lett.* 91 (2007) 092101.
- [20] J. Schörmann, S. Potthast, D.J. As, K. Lischka, *Appl. Phys. Lett.* 89 (2006) 131910.
- [21] D.J. As, S. Potthast, U. Köhler, A. Khartchenko, K. Lischka, *MRS Symp. Proc.* 743 (2003) L5.4.
- [22] M.D. Craven, P. Waltereit, J.S. Speck, S.P. DenBaars, *Appl. Phys. Lett.* 84 (2004) 496.
- [23] N. Grandjean, B. Damilano, S. Dalmaso, M. Leroux, M. Lügt, J. Massies, *J. Appl. Phys.* 86 (1999) 3714.
- [24] E.A. DeCuir Jr., E. Fred, M.O. Manasreh, J. Schörmann, D.J. As, K. Lischka, *Appl. Phys. Lett.* 91 (2007) 041911.
- [25] E.A. DeCuir Jr., M.O. Manasreh, E. Tschumak, J. Schörmann, D.J. As, K. Lischka, *Appl. Phys. Lett.* 92 (2008) 201910.
- [26] L. Shen, R. Coffie, D. Bultari, S.J. Heikman, A. Chakraborty, A. Chini, S. Keller, S.P. DenBaars, U.K. Mishra, *IEEE Elec. Dev. Lett.* 25 (2004) 7.
- [27] S. Rajan, P. Waltereit, C. Poblenz, S.J. Heikman, D.S. Green, S.P. DenBaars, U.K. Mishra, *IEEE Elec. Dev. Lett.* 25 (2004) 247.
- [28] M. Abe, H. Nagasawa, S. Potthast, D.J. As, K. Lischka, *IEICE Trans. Electron.* E89-C (7) (2006) 1057.
- [29] S. Potthast, J. Schörmann, J. Fernandez, D.J. As, K. Lischka, H. Nagasawa, M. Abe, *Phys. Status Solidi C* 3 (6) (2006) 2091.